

# Light Tunable Gratings Based on Flexoelectric Effect in Photoresponsive Bent-Core Nematics

Hongzhen Jing, Mingya Xu, Ying Xiang,\* Everett Wang, Dongfeng Liu, Anna Poryvai, Michal Kohout,\* Nándor Éber, and Ágnes Buka

**A new photoresponsive bent-core nematic (BCN) material, which exhibits flexoelectric domains (FDs) driven by electric field, is reported. Unexpectedly, it is found that the morphologies of FDs can be controlled by irradiation with light fields. This light tunability is ascribed to the photoisomerization effect of the azo moiety within the BCN molecules, where the ratio of *trans* and *cis* isomers changes according to the parameters of the light field, resulting in adjustable electric threshold and periodicity of FDs. Based on this principle, a prototype of controllable optical grating is assembled, whose operation can be manipulated by the wavelength or intensity of light. Due to the easy, instant, and remote operation by light, this optical, contactless tunability has a great advantage over traditional electric control in tunable photonic devices.**

## 1. Introduction

Liquid crystals (LCs) represent a unique class of materials since they combine the long range order of crystals with the mobility of liquids. Besides, the ordered structure (mesophase) can be influenced by temperature (thermotropic LCs) or concentration (lyotropic LCs); additional external stimuli such as mechanical stress, electric, magnetic, and light fields can also be applied to modulate the ordered system. Thanks to these properties, LCs are in daily use in liquid crystal displays (LCDs), optical shutters, or contact thermometers.<sup>[1,2]</sup>

In the last few years, research has been conducted on a new class of LCs, so-called phototropic liquid crystals (PtLCs), whose

properties can be modulated by ultraviolet (UV) and visible light. Such materials could find interesting applications in photonic devices, including optical memories, optical displays, and optical switches.<sup>[3]</sup>

So far, most PtLC materials and their applications have been realized by doping a standard LC with a separate photochromic dye.<sup>[4–9]</sup> However, recently, novel PtLC materials comprising only a single component have been developed, in which every mesogenic molecule of LCs contains a photosensitive moiety.<sup>[10]</sup> In particular, PtLCs containing an azo group in their structure have been widely exploited, as they exhibit both the photosensitivity of

azobenzene compounds and the high birefringence of LCs. The azobenzene moiety plays both the role of the mesogenic core and the photosensitive moiety, and thus, it can be incorporated in calamitic (rod-like), discotic and bent-core PtLCs.

The azobenzene-based LCs usually exhibit mesomorphic behavior, if the azobenzene moiety adopts the linear *trans*-configuration. However, photoisomerization into the *cis*-form leads to bending of the molecule, which induces disorder within the oriented liquid and may trigger isothermal phase transition to the isotropic phase. Besides the order to disorder phase transition, the change in the molecular shape of azobenzene-based molecules upon photoisomerization also influences the physical properties of LCs, such as the dielectric constant<sup>[11]</sup> and elasticity.<sup>[12]</sup> Changing the ratio between the populations of isomers is therefore a very effective way to modify the behavior of PtLCs by means of light.<sup>[13,14]</sup>

Bent-core liquid crystals (BCLCs) are unique materials, since they may exhibit polar order and spontaneous symmetry breaking in ordered liquid crystalline fluids consisting of achiral molecules.<sup>[15,16]</sup> The bent molecular shape causes differences also in other physical properties of BCLCs, such as anomalous anisotropies of elastic constants or a giant flexoelectric effect.<sup>[17–19]</sup> In addition, the introduction of a functional group that allows for the modulation of the properties of BCLCs by means of magnetic field<sup>[20,21]</sup> or light<sup>[20–26]</sup> is nowadays of eminent interest. UV light stimulus can stabilize blue phases;<sup>[27]</sup> it may cause isothermal chirality switching<sup>[25,28]</sup> which results in reversible phototuning of the wave vector of electroconvection patterns in cholesterics.<sup>[4]</sup> Potential applications of BCLC materials, in particular those exhibiting a nematic phase (bent-core nematics, BCNs), are foreseen in optical data storage, holographic media, photonics, or photoalignment of LC matrices, though they have not been realized yet.

H. Jing, M. Xu, Y. Xiang, E. Wang, D. Liu  
School of Information Engineering  
Guangdong University of Technology  
Guangzhou 510006, P. R. China  
E-mail: frank\_xiang68@qq.com, xiangy@gdut.edu.cn

Y. Xiang  
Guangdong Provincial Key Laboratory  
of Functional Soft Condensed Matter  
Guangdong University of Technology  
Guangzhou 510006, China

A. Poryvai, M. Kohout  
Department of Organic Chemistry  
University of Chemistry and Technology Prague  
Technická 5, CZ-16628 Prague, Czech Republic  
E-mail: michal.kohout@vscht.cz

N. Éber, Á. Buka  
Institute for Solid State Physics and Optics  
Wigner Research Centre for Physics  
Hungarian Academy of Sciences  
H-1121 Budapest, Konkoly-Thege Miklós út 29-33, Hungary

DOI: 10.1002/adom.201801790

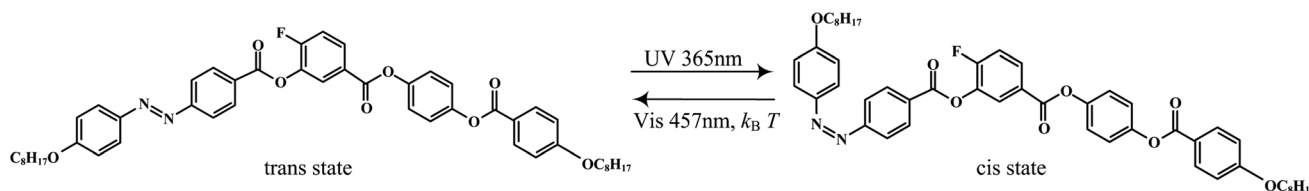


**Figure 1.** Molecular structure of the *trans* (left) and the *cis* (right) isomers of the compound SV775. Photoisomerization changes the geometry of the azobenzene-based molecule; *trans*-to-*cis* isomerization takes place upon exposure to ultraviolet light, whereas the *cis*-to-*trans* back relaxation occurs either when irradiated by visible light or due to thermal relaxation ( $k_B T$ ).

Recently we have synthesized a new BCN material (SV775) bearing an azo linkage, in which both liquid-crystalline and photochromic properties are realized by a single-component azobenzene-based LC molecule. Such an LC material takes full advantage of the high photosensitivity of the azo moiety and the unusual physical properties of the bent-shaped molecular structure. Thus, besides by traditional electric stimuli, it provides complementary opportunity to comprehensively explore modulation of physical properties of BCNs by light stimuli.

The flexoelectric effect (FE) is a physical property characterizing the self-assembly of LC systems; it closely correlates with the molecular structure of LCs.<sup>[29,30]</sup> Induced by elastic deformations (by gradients of the director  $\mathbf{n}$ ), FE manifests itself in an electric polarization,  $\mathbf{P}_f = \epsilon_1 \mathbf{n} \operatorname{div} \mathbf{n} - \epsilon_3 \mathbf{n} \times \operatorname{curl} \mathbf{n}$ , where  $\epsilon_1$  and  $\epsilon_3$  are phenomenological flexoelectric coefficients. When driven by electric field, certain nematics exhibit flexoelectric domains (FDs): a spatially periodic director distortion emerging above a threshold electric voltage  $U_{th}$ .<sup>[31]</sup> In a microscope, they appear as static longitudinal (parallel to the initial orientation  $\mathbf{n}_0$ ) stripes with a periodicity of  $\Lambda$ . FDs emerge as a consequence of the linear coupling between the electric field  $\mathbf{E}$  and the flexoelectric polarization  $\mathbf{P}_f$ .<sup>[30,31]</sup> As a consequence of this linear coupling, FDs are best observable under dc electric field; under ac driving either their threshold voltage increases rapidly with the frequency (for  $f > 1$  Hz), or the director pattern fluctuates with the driving frequency (for  $f < 1$  Hz). The occurrence of FDs is limited to materials whose parameters fulfil specific requirements.<sup>[31,32]</sup> Owing to the combination of the bent molecular shape and a transverse component of dipole moment, BCNs are ideal candidates for compounds exhibiting large flexoelectric coefficients.<sup>[33,34]</sup>

So far, most of the research effort on FDs has been focused on the electrical characteristics of FDs, like the threshold voltage and the voltage dependent periodicity.<sup>[35–37]</sup> Recently, tunability of these characteristics by an additional magnetic field has also been reported;<sup>[38]</sup> nevertheless, the effect of light illumination has not yet been considered. Hereby, we demonstrate that in a photoresponsive BCN system, the behavior of FDs depend on both electric and light fields. Experimental results indicated that  $\Lambda$  as well as  $U_{th}$  of FDs could be changed (increased or decreased), depending on the wavelength  $\lambda$  and intensity  $I$  of the irradiating light.

Our investigation on the properties of FDs induced under the combined action of electric field and light illumination may serve as a guideline to improve the performance of certain photonic devices, for example, via using photoresponsive LCs to achieve an enhanced tunability of electric-field-induced optical

gratings by additional light fields. This unique combination of various stimuli opens new directions in the application of photosensitive BCNs.

## 2. Materials and Experimental Arrangement

### 2.1. Synthesis and Characterization of the Studied Material

The studied BCN material, SV775 (Figure 1) was synthesized according to previously described procedures.<sup>[39,40]</sup> For experimental details see the Supporting Information.

The azobenzene moiety incorporated as a linking unit in one of the rigid arms renders the SV775 molecule photosensitive. It can undergo light-induced isomerization reaction; thus it changes its shape from the bent-core shape of the *trans* isomer (Figure 1, left) into a doubly bent structure of the *cis* isomer (Figure 1, right). In general, the bulk sample consists of both isomers, whose concentration ratio  $C^{cis}/C^{trans}$  depends on the temperature and on the illumination conditions. In the unirradiated ground state the *trans* isomer dominates ( $C^{cis}/C^{trans} \ll 1$ ). UV-vis spectroscopic measurements on the photoisomerization process, as well as additional NMR spectroscopic measurements, providing information on the ratio  $C^{cis}/C^{trans}$  in the ground state and in the photostationary state, on the *cis*-to-*trans* thermal relaxation, and on the effect of irradiation energy on the *trans*-to-*cis* switching rate, can be found in the Supporting Information.

### 2.2. Experimental Arrangement for Observation of Electric- and Light-Field Driven Textures

The SV775 material was filled into standard planar cells with thickness of  $d = 6 \mu\text{m}$ , where the two indium-tin-oxide (ITO) glass substrates were coated with polyimide and rubbed antiparallel to obtain planar alignment  $\mathbf{n}_0$ . The temperature of the samples was controlled using a Linkam LTS420 heating stage with a TMS 94 temperature controller.

dc voltage  $U_{dc}$  from a function generator was applied to the sample via a high voltage amplifier; the resulting electric field was perpendicular to the substrates and  $\mathbf{n}_0$ . The samples were observed by a polarizing microscope (POM) equipped with a white light source and a high resolution CCD camera, in transmission mode at crossed polarizers. In addition, the samples could be irradiated by either UV or visible light from a LED lighter (FUV-8BIT, Height-LED Opto-electronics Technology Co.) with two radiation heads outputting  $\lambda = 365 \text{ nm}$

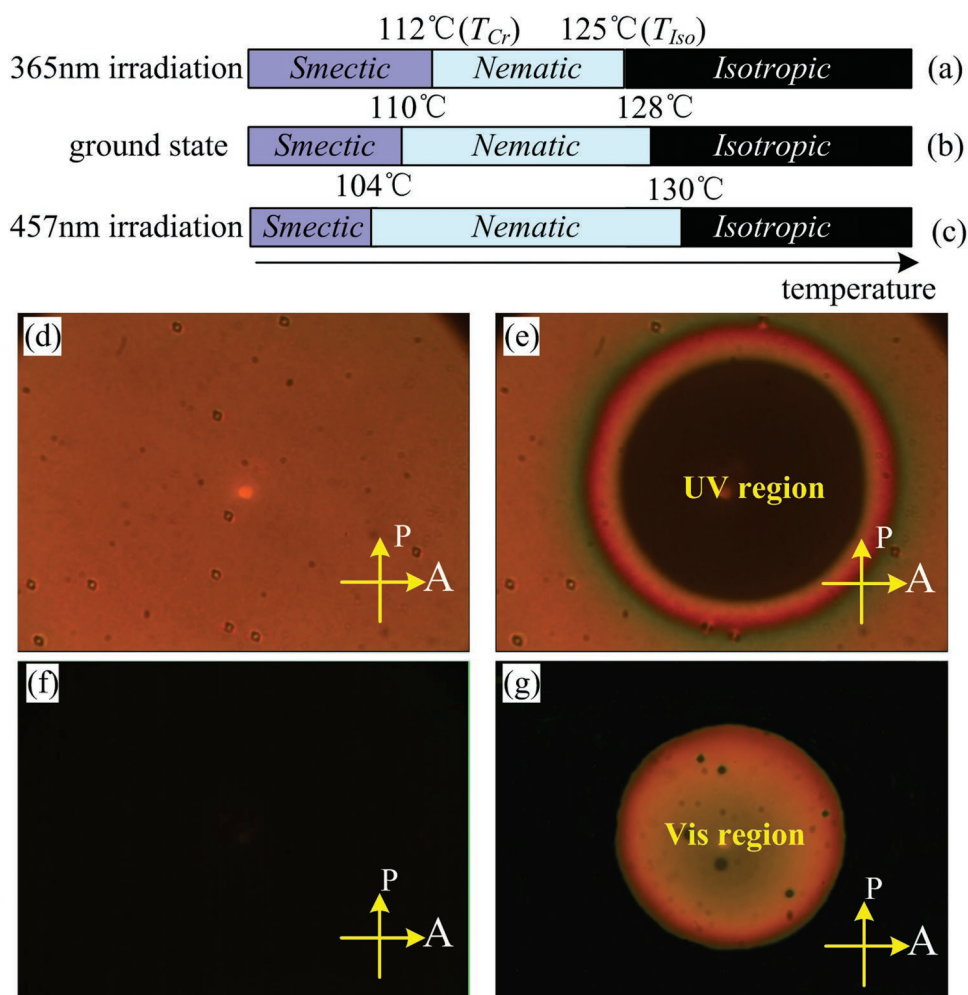


**Figure 2.** Phase diagram of the photochemical phase transitions of SV775 a) under UV light ( $\lambda = 365$  nm) irradiation with  $I_{365} = 4.8$  mW mm<sup>-2</sup>; b) without illumination; c) under visible light ( $\lambda = 457$  nm) irradiation with  $I_{457} = 0.16$  mW mm<sup>-2</sup>; d) without light irradiation, POM micrograph of the nematic phase at  $T = 125$  °C; e) nematic-to-isotropic isothermal transition upon UV 365 nm light irradiation with  $I_{365} = 4.8$  mW mm<sup>-2</sup> for 2 s; f) without light irradiation, POM micrograph of the isotropic phase at  $T = 129$  °C; g) isotropic-to-nematic isothermal transition upon visible 457 nm light irradiation with  $I_{457} = 0.16$  mW mm<sup>-2</sup> for 120 s. After the 457 nm light irradiation was terminated, it took about 3 s for SV775 to return back to isotropic phase. The arrows P and A indicate the directions of the polarizer and the analyzer, respectively.

and  $\lambda = 457$  nm light, respectively; the exciting light was coupled into the POM in reflection mode through a prism. The illuminated area was a circular spot with a diameter of 100  $\mu$ m (see Figure 4e,g); the exposed light intensity could be adjusted by controlling the LED lighter and measured by a UV-B dual-channel irradiation meter positioned on the top surface of the sample. In order to avoid accidental UV content from the white light source, a UV-cut glass filter was used in the POM observation. The textures (patterns) in the samples could be digitally recorded in the absence as well as in the presence of the exciting light.

Besides polarizing microscopy, an independent, optical diffraction technique was also used to probe the characteristics of FDs. The periodic director distortion of FDs corresponds to an optical grating, which diffracts the incident beam of a He-Ne laser ( $\lambda = 633$  nm). The far field diffraction fringes were recorded by a digital camera; from the positions of the diffraction spots the periodicity of FDs ( $\Lambda$ ) was determined.

Sketches of the polarizing microscopy and diffraction setups are presented in Figures S7 and S8, respectively, of the Supporting Information.

### 2.3. Photoisomerization in the Mesophase

The studied BCN exhibits smectic, nematic, and isotropic phases (for details see the Supporting Information). The phase diagrams in Figure 2a–c show that, though the phase sequence is unaffected, the transition temperatures are sensitive to the light illumination due to the *trans*-to-*cis* isomerization of the azo group. If the temperature  $T$  is set inside the nematic phase region ( $T_{Sm} < T < T_{Iso}$ ) and the sample is irradiated with UV light ( $\lambda = 365$  nm),  $T_{Iso}$  will gradually decrease due to the increasing molar fraction of the *cis*-form. Upon reaching a threshold concentration of the *cis*-form,  $T_{Iso}$  becomes lower than  $T$ , which leads to a nematic-to-isotropic

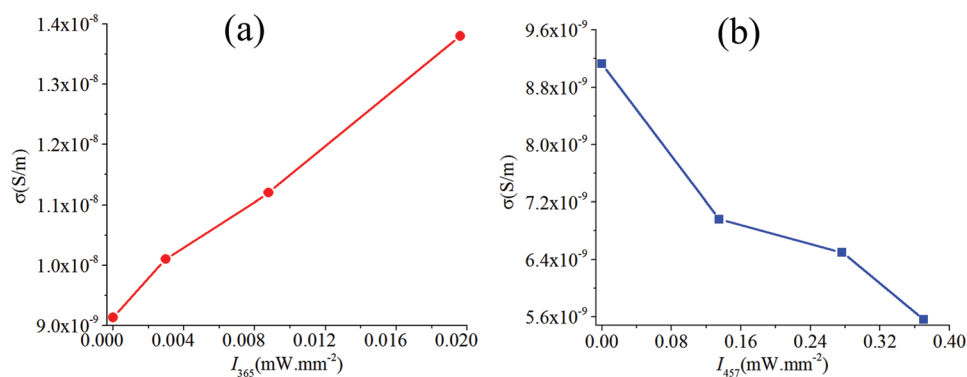


**Figure 3.** Dependence of the electrical conductivity  $\sigma$  on the light intensity  $I$ , a) for illumination with UV light ( $\lambda = 365$  nm) and b) for illumination with visible blue light ( $\lambda = 457$  nm).

phase transition in the illuminated region (Figure 2e). This isothermal phase transition, associated with the increasing *cis/trans* ratio, usually depends on both the UV intensity and the duration of the illumination. Namely, it is the dose (total irradiation energy, the product of light duration and intensity) that controls this process. However, in our case, it was found that the light intensity plays the dominant role in realization of the actual  $T_{\text{Iso}}$ .

Once the illumination is switched off, the population of the *cis* isomer slowly diminishes as the azo unit returns to the thermodynamically more stable *trans*-form. This thermal relaxation process is usually slow and takes typically more than 1 h in the bulk material. However, that process can be accelerated by irradiation with visible light ( $\lambda = 457$  nm), leading to a quick restoration of the nematic phase. Similarly, if the sample is in the isotropic phase (Figure 2f), the application of visible light favors the oriented liquid crystalline state, thus inducing locally an isotropic-to-nematic phase transition (Figure 2g).

While the  $T_{\text{Iso}}$  can be reduced or increased by UV or visible light illumination, respectively, the smectic-to-nematic phase transition temperature exhibits an opposite tendency. Thus, a shrinkage (widening) of nematic temperature range occurs, upon illumination with UV (visible blue) light (Figure 2a–c).

## 2.4. Electrical Conductivity under Illumination

As the patterns investigated are induced by electric field, the electrical conductivity is an important characteristic parameter. We have measured the dc conductivity  $\sigma$  of SV775 in a planar cell at  $T - T_{\text{Iso}}(\text{dark}) = -3$  K, without and under the illumination with UV ( $\lambda = 365$  nm) and visible blue ( $\lambda = 457$  nm) light. The dependence of the conductivity on the illuminating UV and blue light intensity is plotted in Figure 3a,b, respectively. We found that the conductivity increases with respect to its value in dark ( $\sigma \approx 9$  nS m<sup>-1</sup>) under UV illumination, but decreases if illuminated by blue light. The increase (or decrease) of  $\sigma$  is roughly linear within the intensity ranges tested. The total change of the conductivity amounts to about 40–50% of the dark value.

It is well known that the electrical conductivity of liquid crystals originates from their ionic content. We assume that

illumination does not affect the number and the species of the ions, however, it alters the structure (the order parameter) of the nematic matrix, which is also manifested in the changes of the nematic-isotropic phase transition temperature, as shown in Figure 2 above.

We have to note, however, that as we deal with flexodomains, the conductivity of the material is not a relevant parameter (pretending that it is low enough, as in our case). A much higher conductivity of course might prevent the observation of flexodomains, resulting rather in electroconvection.

## 3. Experimental Results

In the following, by keeping the temperature of the samples at  $T - T_{\text{Iso}}(\text{dark}) = -3$  K, the characteristics of FDs under the combined action of dc electric and light fields were examined. A special attention was devoted to the comparison of the influence of irradiating light with different wavelengths on the dc threshold as well as on the morphology of FD patterns.

### 3.1. FDs Driven by dc Field Only

In the absence of light irradiation, the morphologies of FDs depend on the applied dc voltage  $U_{\text{dc}}$ , as illustrated in Figure 4. When  $U_{\text{dc}}$  exceeded the threshold  $U_{\text{th}}^{\text{dark}}$  of the dark state ( $U_{\text{dc}} \geq U_{\text{th}}^{\text{dark}}$ ), FDs emerged in the form of longitudinal stripes running parallel with  $\mathbf{n}_0$ . The snapshots in Figure 4a–d show the FD patterns recorded at successively increasing driving voltage. Their spatial periodicity, the grating constant  $\Lambda$ , obviously decreases upon increasing  $U_{\text{dc}}$ .

Figure 4e plots the voltage dependence of the dimensionless wavenumber  $q = 2 d/\Lambda$  on a relative scale, using the threshold  $U_{\text{th}}^{\text{dark}}$  of the dark state and the critical wave number  $q_{\text{th}}^{\text{dark}}$  at  $U_{\text{th}}^{\text{dark}}$  as scaling units. The dependence is linear, similarly to that of other systems investigated before.<sup>[38]</sup> The measurements presented in Figure 4e were performed at a temperature in the middle of the nematic range. The voltage dependence of the wave number was found to be independent of the temperature within the experimental error.

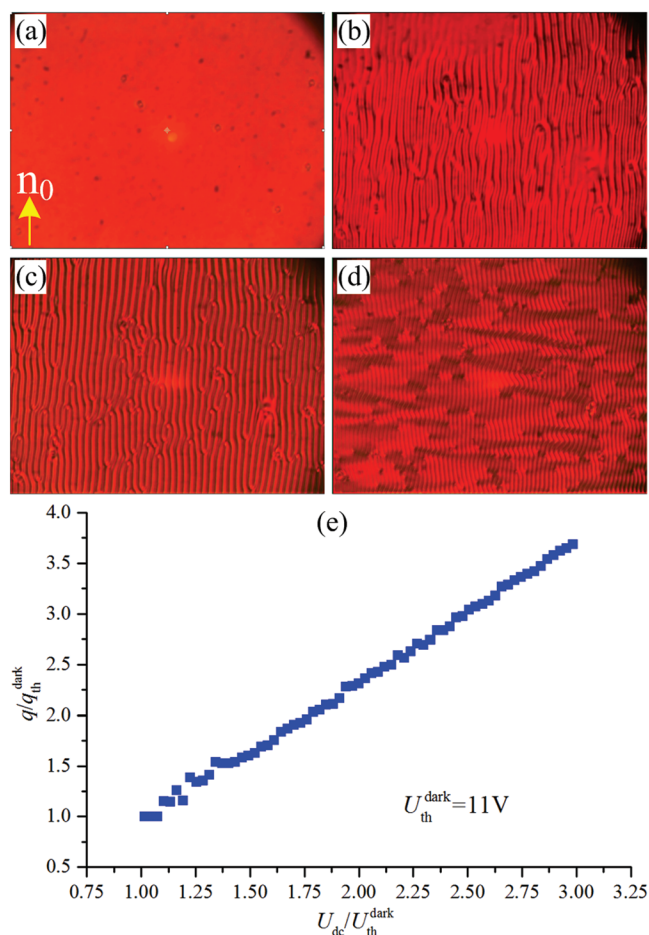


**Figure 4.** Morphologies of FDs under different dc voltages. a)  $U_{dc} = 0$  V; b)  $U_{dc} = U_{th}^{dark} = 11.0$  V and  $\Lambda = 7.7$   $\mu\text{m}$ ; c)  $U_{dc} = 12.0$  V and  $\Lambda = 7.5$   $\mu\text{m}$ ; d)  $U_{dc} = 16.0$  V and  $\Lambda = 5.3$   $\mu\text{m}$ . The size of the snapshots is  $370$   $\mu\text{m} \times 280$   $\mu\text{m}$ . e) Dependence of the relative wave number  $q/q_{th}^{dark}$  on the relative voltage  $U_{dc} = U_{th}^{dark}$ .

### 3.2. The Combined Effect of Light and dc Field on FDs

When illuminated, the behavior of the dc voltage-induced FDs alters as a response to the stimuli of the irradiating light of different wavelength and intensity. In the following micrographs, only the areas located inside the dotted circle were illuminated, whereas the areas outside that circle remained in dark (see Figures 5b and 6b as examples).

#### 3.2.1. FDs under Irradiation with UV Light

The experimental results indicated that both the dc threshold and the grating constant  $\Lambda$  of FDs were affected by UV light. However, the relationship between dc voltage and periodicity still held, like that in Section 3.1, where  $\Lambda$  decreased with increasing  $U_{dc}$ . This fact implies that the irradiation of UV light only changed some parameters of the SV775 compound, whereas the mechanism responsible for FD formation remained unaltered.

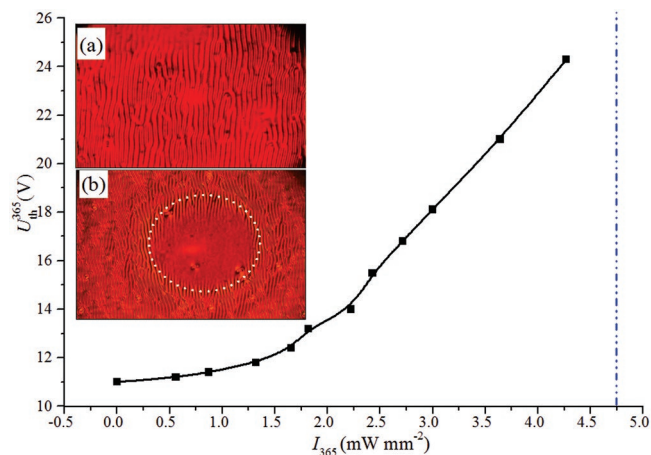


**Figure 5.** Dependence of the threshold voltage  $U_{th}^{365}$  of FDs on the UV intensity  $I_{365}$ . The inset shows snapshots of FDs ( $370$   $\mu\text{m} \times 280$   $\mu\text{m}$ ) a) in the absence of UV illumination ( $I_{365} = 0$   $\text{mW mm}^{-2}$ ) at  $U_{dc} \approx U_{th}^{dark} = 11$  V; b) with a central dotted circular spot after being illuminated by UV ( $I_{365} = 1.6$   $\text{mW mm}^{-2}$ ) for 5 s at  $U_{dc} = 11$  V  $< U_{th}^{365} = 12.4$  V. The dashed-dotted-dotted vertical line marks the critical UV intensity of  $4.8$   $\text{mW mm}^{-2}$ , where the UV-induced nematic to isotropic phase transition occurs.

Depending on the applied voltage and the illumination conditions, we could distinguish the following three cases:

- 1) When  $U_{dc}$  is low, but  $U_{dc} \geq U_{th}^{dark}$  holds, the textures of the samples depend on the light intensity  $I_{365}$ . Without illumination ( $I_{365} = 0$ ), FDs are present uniformly in space, as shown in Figure 5a. In the UV illuminated bright area (inside the dotted circle), the threshold voltage of FDs increased to  $U_{th}^{365} > U_{th}^{dark}$  owing to the irradiation with UV light, as depicted in the graph in Figure 5. As a result, in that region, the applied  $U_{dc}$  is lower than the local threshold

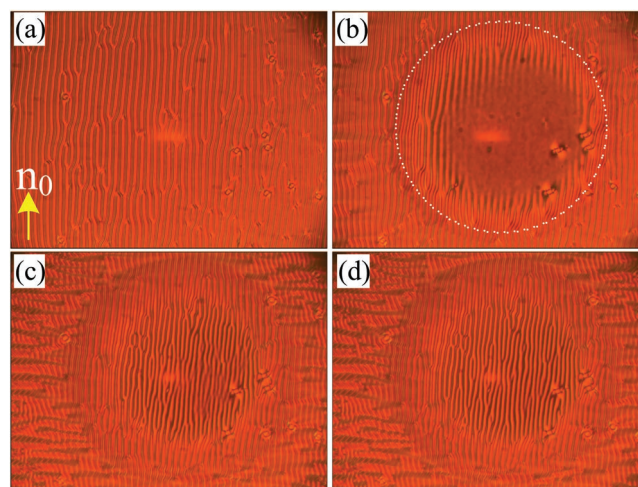


**Figure 6.** Dependence of the FD morphology on the applied voltage  $U_{dc}$  under the same UV intensity. Snapshots ( $370$   $\mu\text{m} \times 280$   $\mu\text{m}$ ) taken a) without UV ( $I_{365} = 0$   $\text{mW mm}^{-2}$ ) at  $U_{dc} = 12.5$  V; under UV intensity of  $I_{365} = 1.1$   $\text{mW mm}^{-2}$  b) at  $U_{dc} = 12.5$  V; c) at  $U_{dc} = 14.0$  V; d) at  $U_{dc} = 15.3$  V.

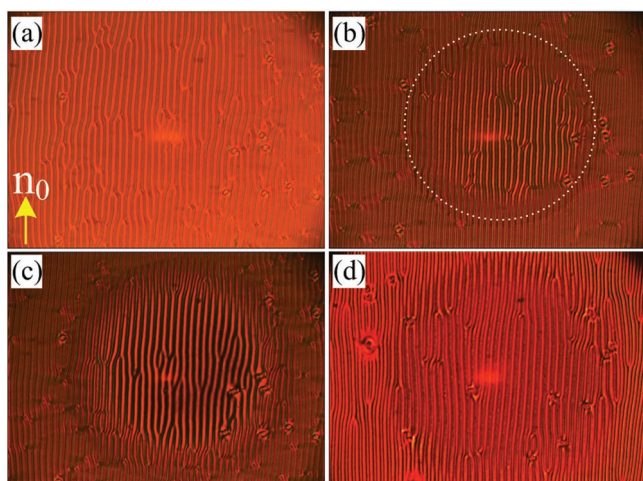


**Figure 7.** Dependence of the FD morphology on the UV intensity at fixed applied voltage of  $U_{dc} = 12.5$  V. The snapshots ( $370 \mu\text{m} \times 280 \mu\text{m}$ ) correspond to the UV intensities and FD grating constants of a)  $I_{365} = 0 \text{ mW mm}^{-2}$ ,  $\Lambda = 7.2 \mu\text{m}$ ; b)  $I_{365} = 0.63 \text{ mW mm}^{-2}$ ,  $\Lambda = 7.5 \mu\text{m}$ ; c)  $I_{365} = 1.1 \text{ mW mm}^{-2}$ ,  $\Lambda = 7.7 \mu\text{m}$ ; d)  $I_{365} = 1.7 \text{ mW mm}^{-2}$ ,  $\Lambda = 8.5 \mu\text{m}$ .

( $U_{th}^{365} > U_{dc} > U_{th}^{dark}$ ), which evidently causes the extinction of FDs (Figure 5b).

In fact,  $U_{th}^{365}$  grew quickly with the increase of  $I_{365}$  and eventually diverged when  $I_{365}$  approached a critical value of  $4.8 \text{ mW mm}^{-2}$  (indicated by the dashed-dotted-dotted vertical line in the graph of Figure 5). Inspection of Figure 2a–e indicates that at the current temperature [ $T - T_{iso}(\text{dark}) = -3 \text{ K}$ ], under that critical UV intensity, the system undergoes an isothermal nematic-to-isotropic phase transition; the nematic phase vanishes and thus FDs disappear resulting in an infinite  $U_{th}^{365}$ .

On the contrary, in the dark area (outside the dotted circle), where the threshold of FDs remains unaffected ( $U_{th}^{dark}$ ) and

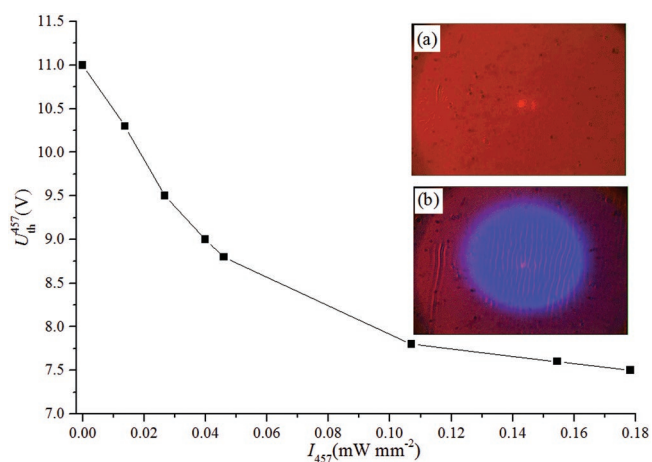


**Figure 8.** The effect of visible light intensity on the FD threshold voltage. The insets show snapshots ( $370 \mu\text{m} \times 280 \mu\text{m}$ ) of FDs a) in the absence of blue illumination ( $I_{457} = 0 \text{ mW mm}^{-2}$ ), where no FDs are present at  $U_{dc} = 10 \text{ V} < U_{th}^{dark}$ ; b) in a central circular spot illuminated by blue light ( $I_{457} = 0.178 \text{ mW mm}^{-2}$ ), where FDs are present at  $U_{dc} = 10 \text{ V} > U_{th}^{457} = 7.5 \text{ V}$ .

therefore lower than the applied  $U_{dc}$ , FDs are present normally, as shown in Figure 5a. Thus, areas with and without FDs coexist in the sample; their spatial distribution is in correlation with the geometry of the irradiating UV light intensity.

- When  $U_{dc}$  is high being in the range of  $U_{dc} < U_{th}^{365} \leq U_{th}^{dark}$ , FDs are present both in the illuminated and unilluminated areas; however, the characteristics of FDs in them are different as shown in Figure 6. In the unilluminated area, the fringes of FDs are denser, with a smaller  $\Lambda$ ; whereas in the illuminated area, the fringes are sparser with a larger grating constant. This spectacular contrast, which persists independent of the actual applied voltage at a given UV intensity (see Figure 6b–d), arises as a consequence of the different threshold voltages in the dark and bright areas.
- Figure 7** illustrates the case, when  $U_{dc}$  is fixed at some higher value and the intensity  $I_{365}$  of the UV irradiation is gradually increased. While the pattern is unaffected in the unilluminated area, the contrast of FDs becomes weaker and their grating constant becomes larger in the illuminated area, where  $I_{365}$  increases. This behavior again can be attributed to the increase of the threshold  $U_{th}^{365}$  ( $I_{365}$ ), which causes the voltage deviation  $U_{dc} - U_{th}^{365}$  (that governs  $\Lambda$ ) to decrease.

### 3.2.2. FDs under the Irradiation with Visible Light

The behavior of FDs can be modified also by visible light, just its effect is opposite to that observed under UV light.

- When  $U_{dc}$  is low and is below the threshold ( $U_{dc} < U_{th}^{dark}$ ), no FDs are present in the unilluminated regions (**Figure 8a**). In the illuminated area, however, the blue light ( $\lambda = 457 \text{ nm}$ ) reduces the threshold voltage to  $U_{th}^{457} < U_{th}^{dark}$  (see the graph in Figure 8); as a result, if  $U_{th}^{457} \leq U_{dc} < U_{th}^{dark}$  fulfils, FDs emerge (Figure 8b). Again, regions with and without FDs coexist in the sample and their spatial distribution is governed by the size and shape of the illumination spot. However, compared with the case described in Section 3.2.1 (irradiation with UV light, Figure 5), here the distribution of FDs is inverted, due to the opposite dependence of the threshold voltage on the light intensity.
- When  $U_{dc}$  is high ( $U_{dc} \geq U_{th}^{dark}$ ), FDs are present uniformly in the unilluminated sample (**Figure 9a**). However, when subjected to blue light, a difference in the behavior of FDs inside and outside the illuminated spot develops (Figure 9b). In the unilluminated area, the fringes of FDs are more spacious corresponding to a larger grating constant  $\Lambda$ ; whereas in the illuminated area, the fringes are denser with a smaller  $\Lambda$ . Reducing  $U_{dc}$  to  $U_{th}^{457}$  ( $I_{457}$ )  $\leq U_{dc} < U_{th}^{dark}$ , FDs disappear in the unilluminated region, while they still persist in the illuminated area (Figure 9c,d). Similar to those aforementioned, this spectacular feature arises from the different threshold voltages in the unilluminated and illuminated areas, as shown in Figure 8.
- When  $U_{dc}$  is fixed at a value of  $U_{dc} > U_{th}^{dark}$  while the intensity  $I_{457}$  of the blue irradiation is increased, FDs in the illuminated area became denser and their grating constant  $\Lambda$  becomes smaller, as shown in the image sequence of **Figure 10**. Again, this is the consequence of the reduction of the threshold

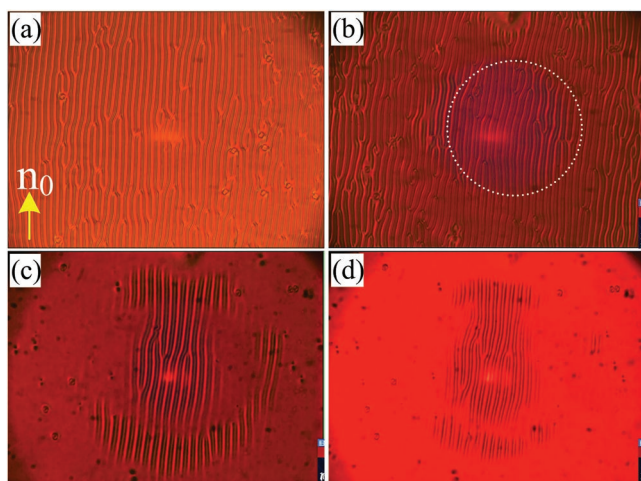


**Figure 9.** Dependence of the FD morphology on the applied voltage  $U_{dc}$  under the same blue light intensity. Snapshots ( $370 \mu\text{m} \times 280 \mu\text{m}$ ) taken a) without blue light ( $I_{457} = 0 \text{ mW mm}^{-2}$ ) at  $U_{dc} = 12.5 \text{ V}$ ; and under  $I_{457} = 0.013 \text{ mW mm}^{-2}$  b) at  $U_{dc} = 12.5 \text{ V}$ ; c) at  $U_{dc} = 10.8 \text{ V}$ ; d) at  $U_{dc} = 10.5 \text{ V}$ .

$U_{th}^{457} (I_{457})$  in the illuminated area, while  $U_{th}^{dark}$  in the unilluminated area does not change.

## 4. Discussion

### 4.1. Tunability of the Phase Diagram of S775 by Light Fields

Being a PtLC material, SV775 molecules exist as either *trans* or *cis* isomers, thus the system is composed of these two isomers. While the bent-shaped *trans* isomers are ordered and form the nematic phase, the W-shaped *cis* isomers favor random positioning and prefer the isotropic phase. Thus the nematic ordering of SV775 comes from the contribution of the *trans* isomers. Namely, the higher the population of the *trans* isomers, the stronger the orientational ordering and the larger the anisotropy of the SV775 system.

When subjected to UV light, *trans* isomer molecules continuously undergo photoisomerization to *cis* isomer molecules, which disorganizes the ordering of the nematic phase. As a result, the clearing temperature  $T_{iso}$  decreases and the temperature range of the nematic phase becomes narrower, as shown in Figure 2a. In extreme cases, when the UV intensity exceeds a threshold value and the resultant concentration of the *cis* isomer is high enough, the system will directly undergo an isothermal transition from the nematic phase into the isotropic phase.

In contrast, when illuminated by visible light, the excited *cis* isomers relax to the *trans* isomers. As the concentration of *trans* isomers increases, the system becomes more ordered, thus  $T_{iso}$  becomes higher and the nematic phase region becomes wider accordingly, as demonstrated in Figure 2c.

### 4.2. The Tunability of FD Morphology by Light Fields

Besides the aforementioned effect on the phase transition, the change of molecular shape upon irradiation also changes

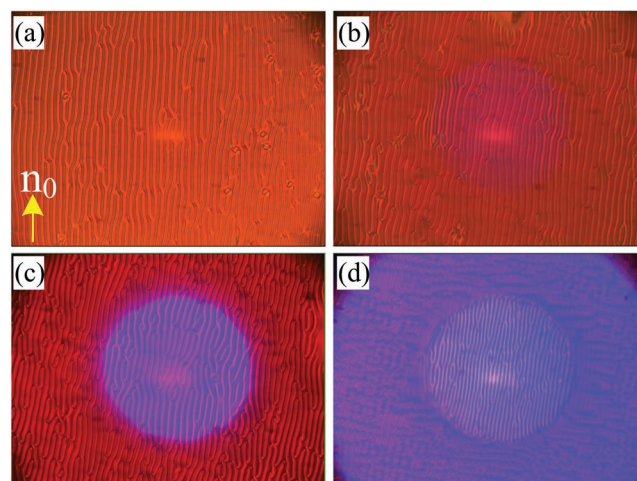


**Figure 10.** Dependence of the FD morphology on the blue light intensity at fixed applied voltage of  $U_{dc} = 12.0 \text{ V}$ . The snapshots ( $370 \mu\text{m} \times 280 \mu\text{m}$ ) correspond to the blue light intensities and FD grating constants of a)  $I_{457} = 0 \text{ mW mm}^{-2}$ ,  $\Lambda = 7.5 \mu\text{m}$ ; b)  $I_{457} = 0.014 \text{ mW mm}^{-2}$ ,  $\Lambda = 6.5 \mu\text{m}$ ; c)  $I_{457} = 0.045 \text{ mW mm}^{-2}$ ,  $\Lambda = 6.3 \mu\text{m}$ ; d)  $I_{457} = 0.178 \text{ mW mm}^{-2}$ ,  $\Lambda = 4.1 \mu\text{m}$ .

the physical properties of SV775. Being a mixture of *trans* and *cis* isomers, the material parameters of the SV775 system are affected by both isomers. However, their contributions are quite different: *trans* isomers are ordered and give rise to the anisotropic properties of the system, whereas *cis* isomers are randomly oriented and promote isotropic behavior. Thus the order parameter as well as the material parameters of the SV775 system depend on the relative population of these two isomers.

In our case, the key factor dominating the evolution of FDs is the threshold voltage  $U_{th}$ , which can be altered by the wavelength as well as the intensity of light. Actually,  $U_{th}$  is an indicator characterizing the anisotropy, which strongly depends on the order parameter  $S$  of the BCN system. According to our experimental results, if  $S$  increases, then  $U_{th}$  decreases; or when  $S$  diminishes,  $U_{th}$  increases. The behavior of  $U_{th}$  changing according to light exposure conditions are summarized as follows:

- 1) When the sample is in its ground state without light stimuli, the population ratio between *trans* and *cis* isomers is determined by the thermal equilibrium. Due to thermodynamic stability, the majority of SV775 molecules exists as *trans* isomers, giving rise to the equilibrium  $S(I=0)$ , which results in the normal threshold  $U_{th}^{dark}$ .
- 2) When irradiated with UV light of  $\lambda = 365 \text{ nm}$ , the molecules adopting *trans*-configuration undergo photoisomerization to the corresponding *cis*-configuration; the population  $C^{trans}$  of *trans* isomer diminishes. The time-dependent molar ratio of *cis* and *trans* isomers under the UV irradiation can be determined from the  $^1\text{H}$  NMR spectra (see Figure S6 and Table S2 in the Supporting Information). The higher the  $I_{365}$ , the lower the  $C^{trans}$ . Thus, the order parameter  $S$  becomes smaller [ $S(I_{365}) < S(I=0)$ ] as  $I_{365}$  increases, which leads to an enhanced threshold  $U_{th}^{365} (I_{365}) > U_{th}^{dark}$ . Furthermore, when  $I_{365}$  increases to a critical value ( $4.8 \text{ mW mm}^{-2}$ ),  $U_{th}^{365}$  diverges,

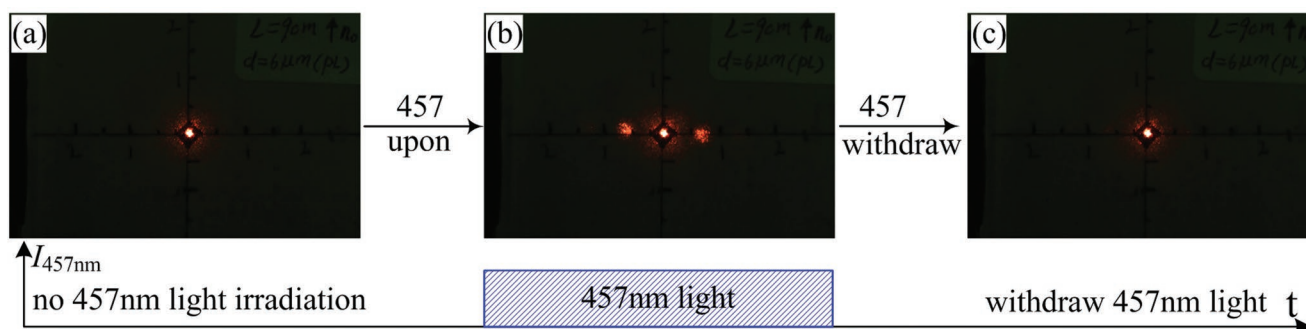


**Figure 11.** Turn on operation controlled via  $\lambda = 457$  nm irradiation, at  $U_{dc} = 12$  V. a) The initial state with only dc voltage applied; b) the grating is present under both dc voltage and  $\lambda = 457$  nm light illumination; c) the grating ceases after the cancellation of the  $\lambda = 457$  nm irradiation, while dc voltage is still on.

implying that the SV775 system undergoes an isothermal nematic-to-isotropic transition and the anisotropy vanishes accordingly, as shown in Figure 5.

- When illuminated with visible light of  $\lambda = 457$  nm, the molecules adopting *cis*-configuration undergo a reverse photoisomerization and relax to the *trans* isomers; then  $C^{trans}$  grows that results in a higher  $S$  [ $S(I_{457}) > S(I = 0)$ ]. Consequently,  $S(I_{457})$  increases for higher  $I_{457}$ , which leads to a reduced threshold  $U_{th}^{457}(I_{457}) < U_{th}^{dark}$ , as shown in Figure 8.

Consequently, as the photochromic reactions are reversible and the two isomers can be interchanged by light irradiation with different wavelengths, the changes of the population ratio between *trans* and *cis* isomers give rise to isothermal differences in the order parameter, which alters the threshold of FDs and modulates the morphologies of FDs.

## 5. Prototype of Photonic Devices and Tunable Operations

The aforementioned tunability of FDs by light fields can be exploited to design new kinds of controllable diffraction gratings. For demonstration we fabricated a prototype device, which controls the direction and the intensity of an incident  $\lambda = 633$  nm (red) light beam. A constant dc voltage  $U_{dc}$  is applied to a planar cell of SV775. Control by light is implemented by illumination of the sample by light beams of  $\lambda = 365$  nm (UV) and  $\lambda = 457$  nm (blue) through appropriate shutters. A sketch of the optical setup is available in Figure S8 in the Supporting Information. Under the proper combination of voltage and UV or blue illumination, the device can realize two functionalities: a shutter functionality (switching on or off the diffracted red light beam) and a beam steering functionality (changing the direction of the red light beam diffracting on the grating). The necessary conditions for these operations are given below.

### 5.1. Shutter Functionality (Switching the Grating On/Off)

#### 5.1.1. Operation #1: Switching the Grating On

Initially, the device is driven by  $U_{dc}$  being in the range of  $U_{th}^{457} < U_{dc} < U_{th}^{dark}$ , to ensure a homogeneous initial state, where

there is no grating, and hence no diffraction (Figure 11a). Once the device is illuminated by blue light, due to the lowering of the FD threshold, the grating appears and diffraction spots are produced (Figure 11b). Afterward, if the blue light is turned off, the grating decays and the diffraction spots disappear (Figure 11c). For an observer along the first order diffracted beam, this operation corresponds to turning the red light on and then off.

Depending on the light intensity, the grating takes several to tens of seconds to form and decay, as demonstrated in Figure 12. Apparently, the stronger the  $I_{457}$ , the faster the forming process, while the slower the decay process. This time evolution behavior strongly correlates with the photoisomerization rate governed by the light intensity.

#### 5.1.2. Operation #2: Switching the Grating Off

The BCN device is driven by  $U_{dc}$  being in the range of  $U_{th}^{dark} < U_{dc} < U_{th}^{365}$ , thus in the initial state the grating (due to FDs) is present; the resulting diffraction spots are depicted in Figure 13a. Once the UV light irradiates the device, the FD

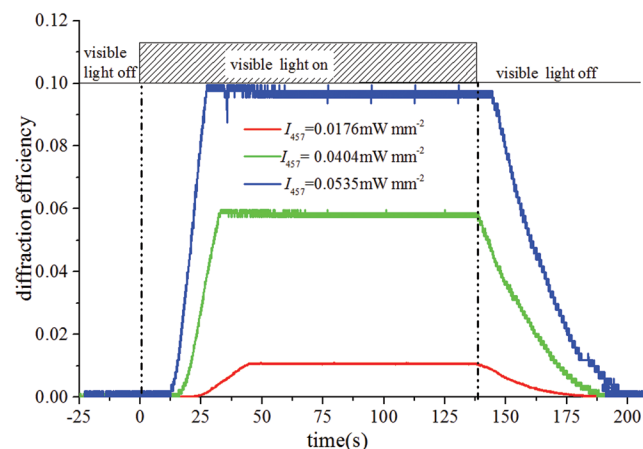


**Figure 12.** Temporal evolution of the first order diffraction efficiencies during the grating switching on process stimulated by blue light of different intensity, at fixed  $U_{dc} = 10.5$  V. The dashed-dotted-dotted lines indicate the moments when the light intensity changes.

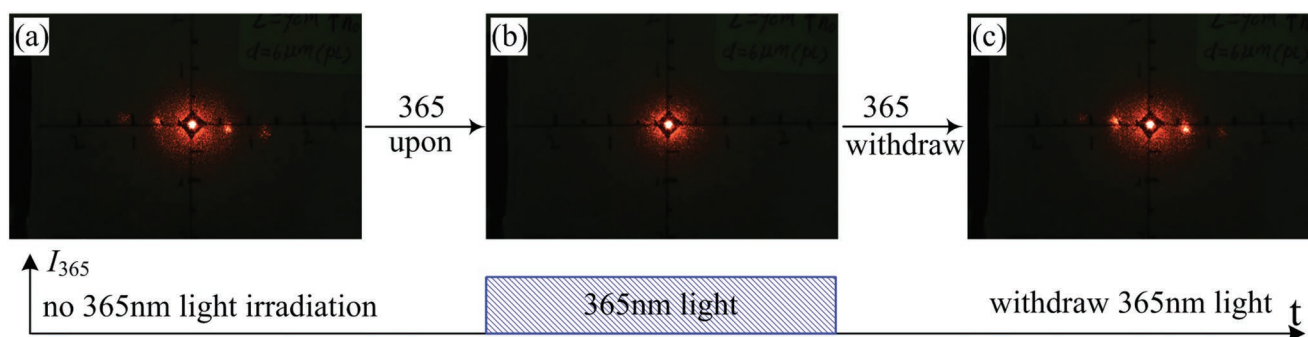


**Figure 13.** Switch-off operation controlled via  $\lambda = 365$  nm UV irradiation. a) The initial state with only dc voltage applied; b) grating is erased under both dc voltage and  $\lambda = 365$  nm light; c) grating is restored after the cancellation of the UV light, while dc voltage is still on.

threshold grows above the applied  $U_{dc}$ , and hence FDs decay and the diffraction spots disappear (Figure 13b). Subsequently, the grating restores after turning off the UV illumination (Figure 13c).

The dynamics of this switch-off operation is illustrated in Figure 14, which proves that it takes several to tens of seconds to finish the decay or recovery process. Similarly to the aforementioned switch-on operation, this time evolution also strongly depends on the UV intensity; the higher  $I_{365}$ , the faster the decay process, while the slower the recovery process. Apparently, with a higher  $I_{365}$ , larger population of the *cis* isomer is produced in a fixed time; afterward it takes more time for them to relax back thermally to the initial *trans* isomer state after the UV light is withdrawn.

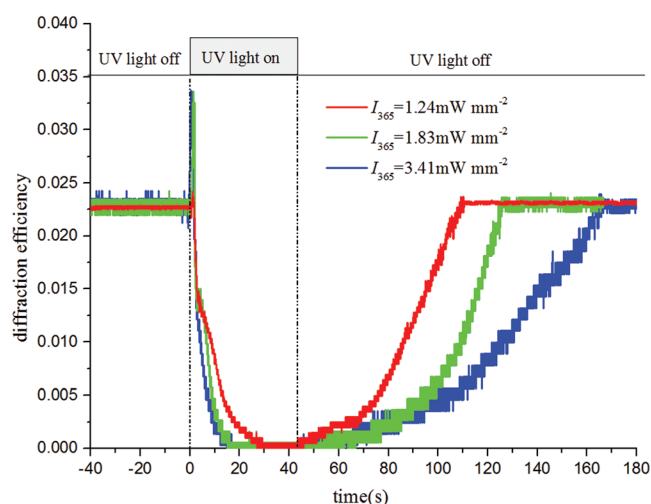


**Figure 14.** Temporal evolutions of the 1st order diffraction efficiencies during the grating switching off process stimulated by UV light with different intensity, at fixed  $U_{dc} = 11.2$  V. The dashed-dotted-dotted lines indicate the moments when the light intensity changes.

## 5.2. Beam Steering Functionality (Controlling the Periodicity of the Grating)

### 5.2.1. Operation #3: Enlarging the Periodicity

Without UV or blue light irradiation, driven by a dc voltage  $U_{dc} > U_{th}^{365} > U_{th}^{dark}$ , the FD grating has a periodicity of  $\Lambda_0$ , as demonstrated by the diffraction spots in Figure 15a. When the device is illuminated by UV light, the FD threshold voltage increases from  $U_{th}^{dark}$  to  $U_{th}^{365} (I_{365}) > U_{th}^{dark}$ . Consequently, the

excess voltage above threshold ( $\Delta U = U_{dc} - U_{th}$ ) diminishes, which results in an enlarged ( $\Lambda_1 > \Lambda_0$ ) periodicity, corresponding to diffraction spots becoming closer to each other as seen in Figure 15b. Furthermore, the resulting grating constant

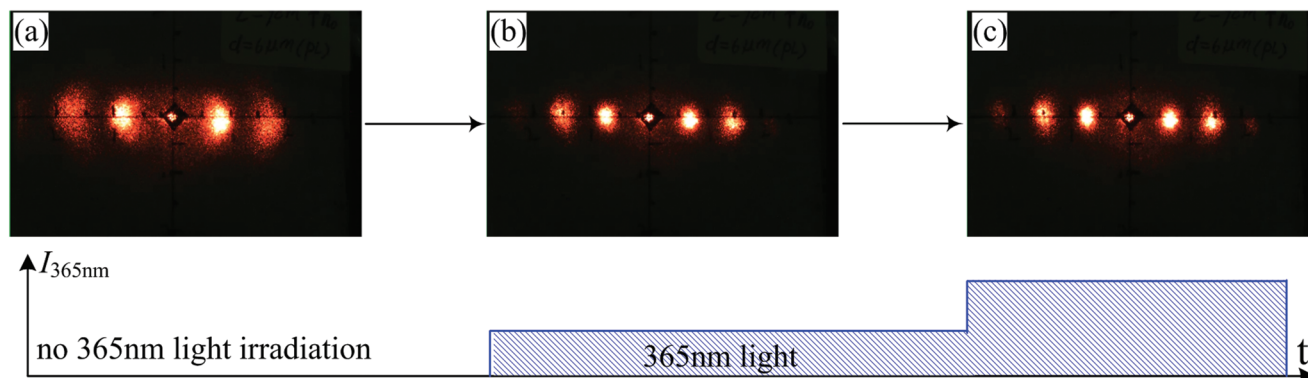


**Figure 15.** Enlarging the grating periodicity, controlled via  $\lambda = 365$  nm irradiation. a) The initial state with only dc voltage applied ( $U_{dc} = 12.5$  V and  $\Lambda_0 = 7.2$   $\mu\text{m}$ ); b) periodicity is enlarged under both dc voltage and UV light ( $I_{365} = 1.1$   $\text{mW mm}^{-2}$  and  $\Lambda_1 = 7.6$   $\mu\text{m}$ ); c) periodicity is enlarged further with a higher intensity UV light ( $I_{365} = 1.28$   $\text{mW mm}^{-2}$  and  $\Lambda_1 = 8.2$   $\mu\text{m}$ ).

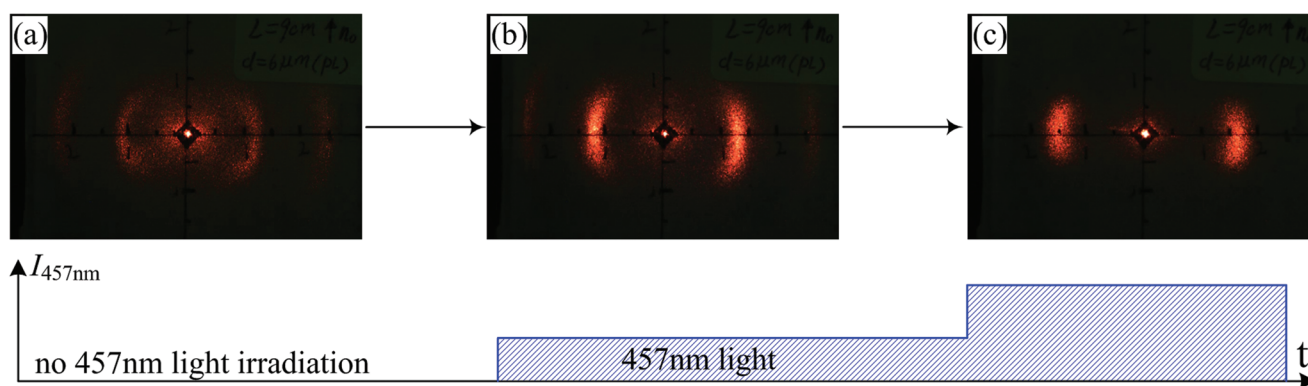


**Figure 16.** Shrinking grating periodicity by irradiation with blue light, where  $U_{dc} = 17$  V. a) The initial dark state with only dc applied ( $\Lambda_0 = 4.6$   $\mu\text{m}$ ); b) periodicity decreases under both dc and blue light ( $I_{457} = 0.014$   $\text{mW mm}^{-2}$  and  $\Lambda_2 = 4.4$   $\mu\text{m}$ ); c) periodicity decreases further with a stronger blue light ( $I_{457} = 0.046$   $\text{mW mm}^{-2}$  and  $\Lambda_2 = 3.5$   $\mu\text{m}$ ).

$\Lambda_1$  of FDs depends on the UV intensity; the higher the intensity of the  $\lambda = 365$  nm light, the larger the grating periodicity (the smaller the distance between the diffraction spots), as seen when comparing Figure 15b with Figure 15c.

#### 5.2.2. Operation #4: Reducing the Periodicity

Without UV or blue light irradiation, driven by a dc voltage  $U_{dc} > U_{th}^{dark}$ , the FD grating has a periodicity of  $\Lambda_0$ , as demonstrated by the diffraction spots in Figure 16a. When illuminated by blue ( $\lambda = 457$  nm) light, the FD threshold voltage  $U_{th}$  decreases from  $U_{th}^{dark}$  to  $U_{th}^{457}$  ( $I_{457} < U_{th}^{dark}$ ); thus the excess voltage above threshold ( $\Delta U = U_{dc} - U_{th}$ ) enlarges, which gives rise to shorter ( $\Lambda_2 < \Lambda_0$ ) periodicity yielding larger separation of the diffraction spots in Figure 16b. A stronger illumination by the blue light yields further reduction of the FD periodicity (larger distance between the diffraction spots), as shown in Figure 16c.

## 6. Conclusion

With the new phototropic BCN material, we observed unusual flexodomains, whose characteristics, such as the dc threshold voltage ( $U_{dc}$ ) and the periodicity (the grating constant  $\Lambda$ ), can be modulated by illumination with light of different wavelength and intensity. This tunability is allowed by the photoisomerization induced change in the ratio of *trans* and *cis* isomers. Such effect of light on the electrically driven optical gratings is a novel phenomenon, which can be used to tune the diffraction properties of gratings. Under illumination with UV light (356 nm), the  $U_{dc}$  increases with increasing intensity of light, which leads to switching off the grating as well as increasing its grating constant. An opposite effect can be achieved by visible light (457 nm), which turns on the grating at given  $U_{dc}$  and also enables increasing the density of the grating.

Based on such optical tunabilities, we fabricated a prototype of diffraction grating device, whose periodicity can be easily

adjusted bidirectionally by light fields. Some characteristics (e.g., the diffraction efficiency) of this prototype might not yet seem attractive; which may partly be owing to the poor alignment and limited illumination area of the prototype cell. We want to emphasize, however, that our main aim in this paper was not device fabrication, but drawing attention to a yet unreported possibility of tuning the properties of flexodomain gratings by optical fields.

While we managed to demonstrate the effect, creating a future commercial device still requires a lot of development work, including selection of a proper phototropic nematic material with enhanced flexoelectrical properties, improvement of surface and pattern alignment, optimization of the cell thickness, etc., which goes far beyond the scope of the present paper. Nevertheless, we anticipate that our method, taking advantage of the easy, instant, precise, and remote tunability by light, will open a new research direction devoted to single component PtLC materials and light-controlled devices.

## Supporting Information

Supporting Information is available from the Wiley Online Library or from the author.

## Acknowledgements

H.J. and M.X. contributed equally to this work. This work was supported by the National Natural Science Foundation of China (Grant No. 11774070), the Guangdong Provincial Science and Technology Plan (Grant Nos. 2016A050502055, 2017A030313036, and 2016A030313698), Guangzhou Municipal Science and Technology Project (Grant No. 201804010444), Czech Science Foundation (Grant No. 16-12150S), and the National Research, Development and Innovation Office (NKFIH) (Grant No. FK 125134).

## Conflict of Interest

The authors declare no conflict of interest.

## Keywords

liquid crystals, microstructures, optically active materials, self-assembly, stimuli-responsive materials

Received: December 23, 2018

Revised: January 16, 2019

Published online:

- [1] V. G. Chigrinov, *Liquid Crystal Devices: Physics and Applications*, Asid'04 Tutorial Notes, Artech House Publishers, Boston, London **1999**.
- [2] J. W. Goodby, P. J. Collings, T. Kato, C. Tschierske, H. F. Gleeson, in *Handbook of Liquid Crystals*, Vol. 8 (Eds: P. Raynes), Wiley-VCH, Weinheim **2012**.
- [3] T. Ikeda, *J. Mater. Chem.* **2003**, *13*, 2037.
- [4] H. Z. Jing, Y. Xiang, M. Y. Xu, E. Wang, J. Wang, N. Eber, A. Buka, *Phys. Rev. Appl.* **2018**, *10*, 014028.
- [5] J. Sun, R. C. Lan, Y. Z. Gao, M. Wang, W. S. Zhang, L. Wang, L. Y. Zhang, Z. Yang, H. Yang, *Adv. Sci.* **2018**, *5*, 1700613.
- [6] P. Z. Sun, Z. Liu, W. Wang, L. L. Ma, D. Shen, W. Hu, Y. Q. Lu, L. J. Chen, Z. G. Zheng, *J. Mater. Chem. C* **2016**, *4*, 9325.
- [7] Y. Shen, Y. C. Xu, Y. H. Ge, R. G. Jiang, X. Z. Wang, S. S. Li, L. J. Chen, *Opt. Express* **2018**, *26*, 1422.
- [8] Z. G. Zheng, B. W. Liu, L. Zhou, W. Wang, W. Hu, D. Shen, *J. Mater. Chem. C* **2015**, *3*, 2462.
- [9] Y. Li, Y. J. Liu, F. Wang, D. Luo, X. W. Sun, *Opt. Express* **2018**, *26*, 23000.
- [10] A. Sobolewska, S. Bartkiewicz, J. Mysliwiec, K. D. Singer, *J. Mater. Chem. C* **2014**, *2*, 1409.
- [11] H. Allinson, H. F. Gleeson, *Liq. Cryst.* **1995**, *19*, 421.
- [12] H. Allinson, H. F. Gleeson, *J. Mater. Chem.* **1995**, *5*, 2139.
- [13] M. Mathews, R. S. Zola, D. K. Yang, Q. Li, *J. Mater. Chem.* **2011**, *21*, 2098.
- [14] L. D. Sio, A. Tedesco, S. Serak, N. Tabiryan, C. Umeton, *Mol. Cryst. Liq. Cryst.* **2012**, *560*, 143.
- [15] T. Niori, T. Sekine, J. Watanabe, T. Furukawa, H. Takezoe, *J. Mater. Chem.* **1996**, *6*, 1231.
- [16] D. R. Link, G. Natale, R. Shao, J. E. Maclennan, N. A. Clark, E. Körblova, D. M. Walba, *Science* **1997**, *278*, 1924.
- [17] J. Harden, B. Mbang, N. Éber, K. Fodor-Csorba, S. Sprunt, J. T. Gleeson, A. Jákl, *Phys. Rev. Lett.* **2006**, *97*, 157802.
- [18] A. Jákl, *Liq. Cryst. Rev.* **2013**, *1*, 65.
- [19] A. Jákl, O. D. Lavrentovich, J. V. Selinger, *Rev. Mod. Phys.* **2018**, *90*, 045004.
- [20] M. Jasiński, D. Pocięcha, H. Monobe, J. Szczytko, P. Kaszyński, *J. Am. Chem. Soc.* **2014**, *136*, 14658.
- [21] K. Bajzík, M. Kohout, J. Tarábek, J. Svoboda, V. Novotná, J. Vejpravová, D. Pocięcha, E. Gorecka, *J. Mater. Chem. C* **2016**, *4*, 11540.
- [22] M. Alaasar, M. Prehm, C. Tschierske, *Chem. Commun.* **2013**, *49*, 11062.
- [23] M. Alaasar, M. Prehm, K. May, A. Eremin, C. Tschierske, *Adv. Funct. Mater.* **2014**, *24*, 1703.
- [24] N. Trisovic, J. Antanasijević, T. T. Katona, M. Kohout, M. Salamonczyk, S. Sprunt, A. Jakl, K. F. Csorba, *RSC Adv.* **2015**, *5*, 64886.
- [25] M. Alaasar, M. Prehm, Y. Cao, F. Liu, C. Tschierske, *Angew. Chem., Int. Ed.* **2016**, *55*, 312.
- [26] M. Alaasar, *Liq. Cryst.* **2016**, *43*, 2208.
- [27] H. C. Jeong, K. V. Le, M. J. Gim, S. T. Hur, S. W. Choi, F. Araoka, K. Ishikawa, H. Takezoe, *J. Mater. Chem.* **2012**, *22*, 4627.
- [28] M. Alaasar, S. Poppe, Q. Dong, F. Liu, C. Tschierske, *Angew. Chem., Int. Ed.* **2017**, *56*, 10801.
- [29] R. B. Meyer, *Phys. Rev. Lett.* **1969**, *22*, 918.
- [30] Á. Buka, N. Éber, *Flexoelectricity in Liquid Crystals. Theory, Experiments and Applications*, Imperial College Press, London **2012**.
- [31] S. A. Pikin, *Structural Transformations in Liquid Crystals*, Gordon and Breach Science Publishers, New York **1991**.
- [32] A. Krekhov, W. Pesch, A. Buka, *Phys. Rev. E* **2011**, *83*, 051706.
- [33] M. Y. Xu, M. J. Zhou, Y. Xiang, P. Salamon, N. Éber, Á. Buka, *Opt. Express* **2015**, *23*, 15224.
- [34] S. Kaur, V. P. Panov, C. Greco, A. Ferrarini, V. Gortz, J. W. Goodby, H. F. Gleeson, *Appl. Phys. Lett.* **2014**, *105*, 223505.
- [35] Y. Xiang, H. Z. Jing, Z. D. Zhang, W. J. Ye, M. Y. Xu, E. Wang, P. Salamon, N. Éber, Á. Buka, *Phys. Rev. Appl.* **2017**, *7*, 064032.
- [36] D. M. Xu, G. J. Tan, S. T. Wu, *Opt. Express* **2015**, *23*, 12274.
- [37] H. W. Chen, G. J. Tan, Y. G. Huang, Y. S. Weng, T. H. Choi, T. H. Yoon, S. T. Wu, *Sci. Rep.* **2017**, *7*, 39923.
- [38] P. Salamon, N. Eber, A. Buka, T. Ostapenko, S. Dolle, R. Stannarius, *Soft Matter* **2014**, *10*, 4487.
- [39] M. Kohout, J. Svoboda, V. Novotná, D. Pocięcha, M. Glogarová, E. Gorecka, *J. Mater. Chem.* **2009**, *19*, 3153.
- [40] M. Kohout, V. Kozmík, M. Slabochová, J. Tůma, J. Svoboda, V. Novotná, D. Pocięcha, *Liq. Cryst.* **2015**, *42*, 87.